CHALMERS
UNIVERSITY OF TECHNOLOGY

UNIVERSITY OF GOTHENBURG

Active feedback control of photonic molecule microcombs

Master's thesis in Embedded electronic system design

Anton Lööf

Department of Computer Science and Engineering
CHALMERS UNIVERSITY OF TECHNOLOGY
UNIVERSITY OF GOTHENBURG
Gothenburg, Sweden 2022

Master's thesis 2022

Active feedback control of photonic molecule microcombs

ANTON LÖÖF

UNIVERSITY OF
GOTHENBURG

CHALMERS
UNIVERSITY OF TECHNOLOGY

Department of Computer Science and Engineering
Chalmers University of Technology
University of Gothenburg
Gothenburg, Sweden 2022

Active feedback control of photonic molecule microcombs

ANTON LÖÖF

Supervisor: Victor Torres Company, Microtechnology and Nanoscience, Photonics Laboratory
Examiner: Per Larsson-Edefors, Department of Computer Science and Engineering

Master's Thesis 2022
Department of Computer Science and Engineering
Chalmers University of Technology and University of Gothenburg
SE-412 96 Gothenburg
Telephone +46 31 772 1000

Typeset in LaTeX
Gothenburg, Sweden 2022

Active feedback control of photonic molecule microcombs

ANTON LÖÖF
Department of Computer Science and Engineering
Chalmers University of Technology and University of Gothenburg

Abstract

Frequency combs generate coherent and evenly spaced spectral lines. This enables applications within optical communication, for wavelength division multiplexing; metrology, for measuring time and frequency; spectroscopy, for probing a sample at multiple frequencies at the same time, and more. One novel implementation of these devices consists of two coupled resonators in a planar integrated Si_3N_4 platform. The device, called a photonic molecule, generates a coherent frequency comb by four wave mixing from a single input laser. A frequency comb generated by this device has been actively stabilized by thermal control of the pump to resonator detuning.

The feedback system measures the generated comb power and changes the temperature of the resonators, via integrated heaters, to thermo-optically alter the location of the longitudinal modes of the coupled resonators. This changes the detuning such that the converted power remains constant. The control system is evaluated by measuring the stability and phase noise of the repetition rate of the comb. Long term stability is found to increase five-fold with the controller enabled and phase noise is improved by 5 dB for offset frequencies within the integrating bandwidth of the controller compared to a free-running comb in the same state.

These results enable the use of photonic molecules for spectroscopy by increasing the stability of the comb as well as for optical communication by reducing phase noise. The results also make the photonic molecule easier to work with as it becomes less sensitive to environmental effects.

Keywords: Photonic molecule, Microcomb, Feedback Control, FPGA

Acknowledgements

My greatest thanks goes to Israel for his introduction to and assistance in the lab. Without his help would some experiments have taken at least twice as long. I'd also like to thank my supervisor Victor for his ideas, insight and feedback throughout the thesis and my girlfriend Trice for her moral support. Another two thanks goes to Fahmi and Dyako whose proof reading found many errors. Finally I'd like to thank the four heaters and one waveguide that I broke during this thesis for their brave sacrifice.

Anton Lööf, Gothenburg, June 2022

Contents

Abbreviations

ADC Analogue to Digital Converter. 21–24, 27

CW Continuous Wave. 2

DAC Digital to Analogue Converter. 21–23

EOM Electro-Optic Modulator. 17
ESA Electrical Spectrum Analyser. 17, 22

FPGA Field Programmable Gate Array. 35
FSR Free Spectral Range. 7, 11, 15, 20
FWM Four Wave Mixing. 10, 11

GPS Global Positioning System. 16, 17, 27, 28

OEDC Optoelectric Downconversion. 15, 17, 22, 28–30, 33, 34
OSA Optical Spectrum Analyser. 22

PC Personal Computer. 24
PD Photodiode. 12, 15, 17, 22, 24, 34
PID Proportional-Integral-Derivative. I, II, 13, 14, 21–23, 25–27

RF Radio Frequency. 1, 15, 16, 34
RP Red Pitaya. I, II, 21–23, 27, 35

1

Introduction

Optical frequency combs provide a means of connecting traditional microwave sources, like crystal oscillators, with traditional optical sources, like lasers, by generating multiple equidistant lines in the frequency domain [1, 2]. This connection is bidirectional, meaning that a comb can produce a microwave clock from an optical reference as well as the other way around [3]. Using a comb to down-convert an optical source to a microwave frequency gives a relative stability that exceeds that of the best cesium clocks, which account for the current definition of time [2, 3, 4, 5].

The high accuracy of the comb makes it useful in multiple areas where precise measurements of time, frequency or length are needed, such as metrology [4], spectrometry [6, 7, 8], astronomy [9] and radio frequency (RF) synthesis [10]. One could even use two correlated frequency combs to coherently measure the phase and amplitude response of a substance [11, 12, 13]. The multiple equidistant frequency lines are also of use for wavelength division multiplexing in optical communications [14, 15, 16].

However, commercially available fiber frequency combs are expensive, large and feature repetition rates in the Radio Frequency (RF) regime [5, 17]. Some applications, such as optical synthesis [18], benefit from repetition rates above RF [3] and new applications in lidar and integrated metrology could emerge if the physical size of the comb generating device decreases [19]. Increased repetition rate and reduced size can be achieved by implementing a comb on chip; a microcomb [19]. A low noise soliton microcomb balances nonlinearity and dispersion as well as loss and input power in an optical resonator. This leads to a repetition rate defined by the geometry and materials of the chip and not the speed of the driving electronics [19]. However, such a system would still need external equipment such as a pump laser and stabilizing control electronics.

An issue with traditional microcombs is that the conversion efficiency is either low [20] or pose limits in design parameters [21, 22]. This is because the formation of a comb requires pumping the resonator off resonance [23, 24, 22] which means that only a portion of the power can couple to the resonator. Reference [22] solves this by coupling two resonators of different sizes as shown in Figure 1.1, which allows a comb to form while coupling a larger proportion of power into the system compared to a single microresonator. The dual ring system is called a photonic molecule, because of its similarity to molecules [25], and allows for a higher conversion efficiency [22, 26] at the cost of a more complicated system [22]. The molecule seen in Figure 1.1 also contains integrated heaters, which enable control of the resonators by the thermo-

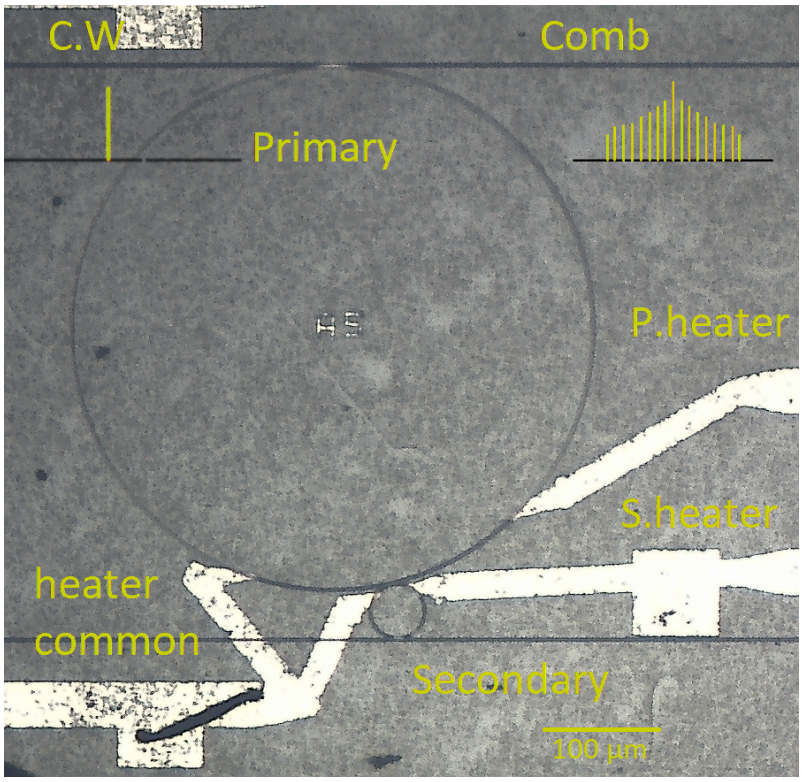

Figure 1.1: Image of photonic molecule. Two ring resonators, primary and secondary, fabricated in Si_3N_4 are shown alongside an input and output waveguide. Connection points for both primary and secondary heater as well as a common ground are highlighted in the figure. The secondary ring is much smaller than the primary ring. The input waveguide is located in the top left of the figure and fed with a continuous wave laser. If the conditions are right, a comb is generated and output via the top right waveguide. Continuous Wave (CW).

optic effect [22].

The long term stability and phase noise of the microcomb is necessary both for understanding its noise performance limits as well as its use in applications. Phase noise is a limiting factor for the bit rate in communication system whereas long term stability is important for metrology and spectroscopy which require long integration time. A critical parameter that characterizes a soliton microcomb is its detuning δ, which corresponds to how far off resonance the resonator is pumped [24, 27]. The detuning is the difference between the frequency of the pump laser and the adjacent resonant frequency, or longitudinal mode, of the resonator. To achieve a long term stable comb, one of these parameters, the mode location or the pump frequency, must be actively tuned to account for variations in the other.

1.1 Goal

The goal of the thesis is to stabilize an initiated soliton microcomb in order to reduce phase noise, increase stability and reduce impact of external disturbances enabling longer and less noisy experiments.

Similar stabilization systems have been developed previously [28, 29]. However, these systems modulate the pump laser frequency to achieve stability. This is a disadvantage since this acts directly onto one of the degrees of freedom in the comb spectrum [30]. This in turn makes it difficult to implement applications where multiple combs have to be derived from the same optical source such as dual comb spectroscopy [13].

1.2 Constraints

The thesis project is constrained by the following constraints:

- The project uses an off the shelf development board, a STEMLab 125-14 [31], as controller
- The project uses prefabricated photonic molecules in a low loss Si_3N_4 platform [32]
- Stability and noise reduction in combs will be achieved by active control, not by engineering an intrinsically better device
- The project will not lock any output from the comb to a frequency reference as demonstrated by [30]

1.3 Thesis outline

The report is divided into five chapters. The second chapter presents relevant theory in order for the reader to understand the following content. The third chapter explains the methods used to solve the problem while the fourth chapter presents the results from solving the problem. The report is finished with a conclusion of the work done and potential future work in the fifth chapter.

2

Theory

The intended audience of this thesis is a student studying embedded electronic design as well as researchers working with microcombs. Here relevant theory is listed such that this audience is easily able to understand the utilized methods, implemented system and final results.

2.1 Light propagation in optical waveguides

Planar electromagnetic waves, $E = E_0 \exp(i\beta(\omega)z)$, where z is the direction of propagation, are the basis of many concepts that are used throughout this thesis. The propagation constant β is of particular interest. It relates to the refractive index of the material that the wave propagates, as seen in Equation 2.1. The effective index n is a function of optical angular frequency ω because the dielectric constant varies with frequency which in turn varies because of resonances in the molecular structure of the atoms of the dielectric. This relation is commonly Taylor expanded.

$$\beta = \frac{\omega n(\omega)}{c} = \beta_0 + \beta_1(\omega - \omega_0) + \beta_2(\omega - \omega_0)^2/2 + \mathcal{O}(\omega - \omega_0)^3 \tag{2.1}$$

One of the terms in Equation 2.1 requires extra attention, β_2 or the group velocity dispersion. It causes different frequencies to propagate at different speeds resulting in a broadening of an incoming broadband pulse. Dispersion is split into two categories, $\beta_2 > 0$ defines normal dispersion which account for the case when high frequencies propagate slower than slow frequencies and $\beta_2 < 0$ defines anomalous dispersion, resulting in the opposite effect.

Light must be confined and directed inside a chip for on chip photonics which is achieved by a dielectric waveguide. An electromagnetic field is guided by a waveguide if its effective index n_e is between the refractive index of the core and cladding of the waveguide. Multiple pairs of fields E_{xy}, H_{xy} satisfy this requirements. These fields are commonly expressed as a sum of the eigenfields or modes of the waveguide. The eigenvalue of the mode is its propagation constant $\beta(\omega) \propto n_e$ from which dispersion is calculated.

These eigensolutions are found numerically using a finite element solver for each geometry. Figure 2.1 shows the power distribution of a mode propagating in a buried waveguide. Notice that the majority of the power propagates inside the core and thus interacts with the core material. The linear and nonlinear properties of this material are important for the creation of optical circuits.

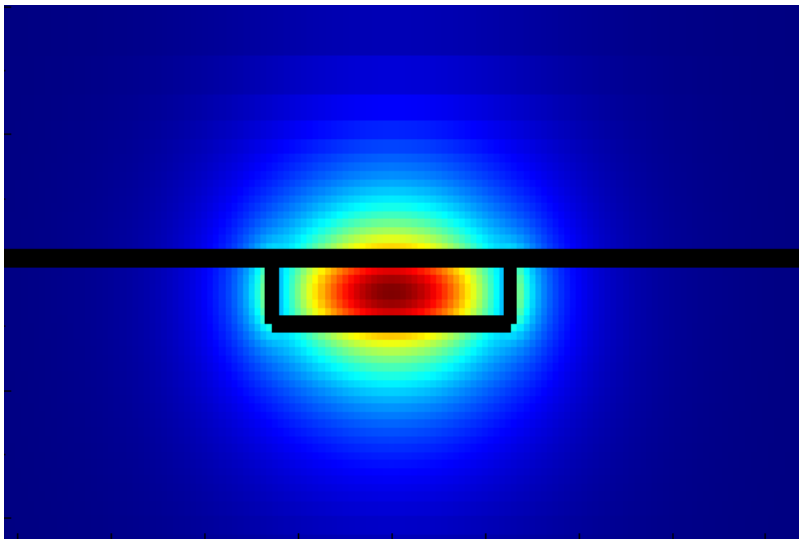

Figure 2.1: Cross section of buried waveguide with simulated mode power distribution for a first order mode. The top and bottom cladding are made from SiO_2 and the core is Si_3N_4. Light propagates in the longitudinal direction, z. The core carries a large amount of power while the cladding carries a smaller amount. Different geometries allow for different proportions of the power to propagate inside the core and cladding.

2.2 Microresonators

Microresonators are the fundamental building blocks that microcombs are built on. For the reader to understand microcombs some aspects of a microresonator must be explained. A drawing of a microresonator is shown in Figure 2.2. It consists of a bus waveguide coupled to a closed loop. Light entering the bus gets coupled to the loop and if the phase of the light coupled from bus to loop matches the phase of the light propagating in the loop the fields will constructively interfere and the power inside the cavity increase. The frequencies for which this constructive interference occurs depends on the phase delay of the resonator which in turn depends on β. These frequencies are called the longitudinal modes of the resonator.

The dynamics of a resonator is formally explained by a two by two coupler at the bus/loop interface, with coupling coefficients t, r, and the propagation delay in the ring, E_a, E_b, as shown in Figure 2.2. A two by two coupler splits the field from two incoming ports between two outgoing ports according to its coupling matrix. The coupling matrix for a lossless coupler is given in Equation 2.2. Propagation inside the ring waveguide is described by Equation 2.3 where L is the length of the loop, α the loss and β the propagation constant.

$$\begin{bmatrix} E_{out} \\ E_a \end{bmatrix} = \begin{bmatrix} t & ir \\ ir & t \end{bmatrix} \begin{bmatrix} E_{in} \\ E_b \end{bmatrix} \tag{2.2}$$

$$E_b = E_a \exp(-\alpha L) \exp(i\beta\omega) = E_a \alpha' \exp(i\beta\omega) \tag{2.3}$$

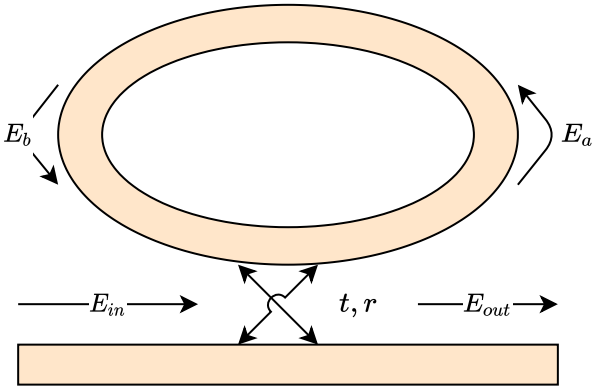

Figure 2.2: Schematic of a microring resonator, two waveguides one straight and one round are coupled at a single point with the coupling coefficients t, r. The electric field at different locations is related by Equations 2.2 and 2.3.

Solving Equations 2.2 and 2.3 for the power transmission yields Equation 2.4, which is a periodic function whose minima corresponds to the longitudinal modes of the resonator where a large proportion of the pump power circulates inside of the cavity.

$$T_{through} = \left(\frac{E_{out}}{E_{in}}\right)^2 = \frac{t^2 + \alpha'^2 - 2t\alpha' \cos \beta L}{1 + t^2\alpha'^2 - 2t\alpha' \cos \beta L} \tag{2.4}$$

Equation 2.5 is an expression, derived from Equation 2.4, for the longitudinal modes, where l is an integer called the longitudinal mode number. The distance between two longitudinal modes gives the resonator Free Spectral Range (FSR) which is a commonly utilized parameter to describe the length of resonators. The resonators used in this thesis will feature an FSR $f_{fsr} = 50\,\text{GHz}$ which corresponds to a ring radius in the order of 200 µm [22, 32].

$$L\beta(\omega_l) = 2\pi l \tag{2.5}$$

The maximum amount of power that can be built up inside the cavity depends on the losses of the cavity as well as the pump power. The cavity losses are characterized by the quality factor $Q = \omega\tau$ of the cavity where τ is the expected photon lifetime inside the cavity [3]. The cavities utilized in this thesis are of $Q \geq 1 \times 10^6$ [32, 22] which result in a large number of photons inside the cavity and thus sufficient buildup of power inside to enable nonlinear effects at low input powers [3].

2.2.1 Coupled microresonators

Two or more microresonators can be coupled to create a system of coupled microresonators. If the longitudinal modes of the resonators are sufficiently close, new longitudinal modes are generated by the interaction of the fields between the resonators [22]. These new modes are given by Equation 2.6 [22] where $\omega_{p,n}$ is the n-th mode of the primary resonator, $\omega_{s,m}$ is the m-th mode of the secondary resonator and κ is the coupling coefficient which depends on the geometry of coupling interface between the resonators. The longitudinal modes given by Equation 2.6 are the

longitudinal modes that should be excited in order to generate a frequency comb in the resonator.

$$\omega_{s,a} = \frac{\omega_{p,n} + \omega_{s,m}}{2} \pm \sqrt{\frac{(\omega_{p,n} - \omega_{s,m})^2}{4} + |\kappa|^2} \tag{2.6}$$

2.2.2 Thermal dependence

As a sweeping pump laser approaches a longitudinal mode of a resonator, more and more power is coupled into the resonator. This results in more power loss inside the resonator some of which is absorbed by the device and heats the device up. The thermo-optic effect then changes the refractive index of the materials inside the waveguide that changes the propagation constant, β, of the mode propagating inside the resonator [33]. A different propagation constant results in a different set of longitudinal modes through Equation 2.5. The thermo-optic effect in Si_3N_4 is positive [34] which shifts the longitudinal modes to a lower frequency.

The thermal shift in longitudinal modes has a different effect on the system depending on from which direction, in frequency, the longitudinal mode was approached from. The shift causes less power to be coupled into the resonator which decreases the temperature and a stable system is achieved if the mode is approached from the blue side (lower wavelength, higher frequency). However, if the approach is made from the red side, more power is coupled into the resonator causing even more drift of the modes and instability [29].

This effect also influences the shape of the resonance. Normally a resonator exhibits a Lorentzian transmission spectrum [33]. However, because of thermal effects this is not the case and the resonance tunes red as more power is coupled into the resonator. This phenomena is described by Equation 2.7 [33]. ΔT is the temperature difference between the resonator and ambient, C_p the heat capacity of the resonator, I_h a measure of dissipated power inside the resonator, λ_0 the cold resonance wavelength, λ_p the pump wavelength, α the coefficient of the combined effect of thermo-optic and thermo-elastic effects on the resonant wavelength, $\Delta\lambda$ the linewidth of the resonance and k the thermal conductivity between resonator and ambient.

$$C_p\dot{\Delta T} = \frac{I_h}{\frac{\lambda_p - \lambda_0(1+\alpha\Delta T)}{\Delta\lambda/2}^2 + 1} - k\Delta T \tag{2.7}$$

2.3 Kerr nonlinearity

The fundamental principle behind microcomb initiation and one of the four balancing effects in stable soliton operation is nonlinearity. The refractive index of a material is dependent on the intensity of the incoming light according to Equation 2.8 where n_1 is the low field refractive index, n_2 is the Kerr coefficient and I ($\mathrm{W\,m^{-2}}$) the intensity of the incoming field [3, 19]. In the context of microcombs, the Kerr nonlinearity is responsible for creating the new frequencies that make up the lines of the comb.

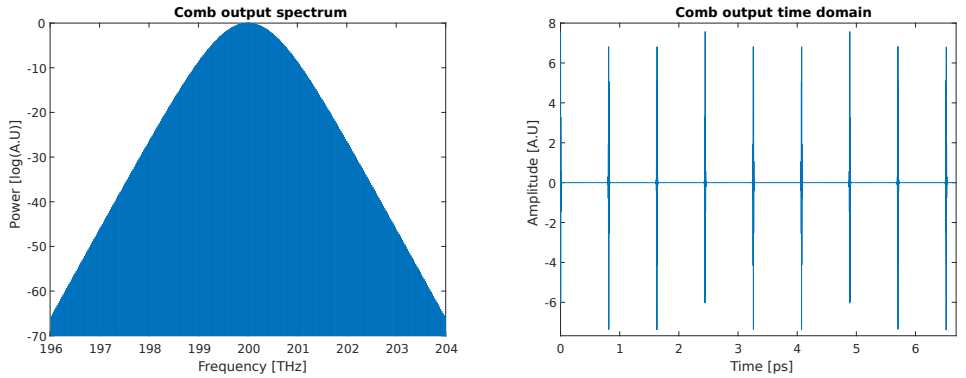

Figure 2.3: Typical spectral and temporal shape of a frequency comb. The left figure shows the frequency domain where evenly spaced phase coherent pure frequencies cover the bandwidth of the comb. The right figure shows the time domain representation. It is a train of pulses that repeat with the same frequency as the distance between the lines in the frequency domain. The pulses act as an envelope on top of the fundamental optical frequency and repeat with the line spacing of the comb.

$$n = n_1 + In_2 \tag{2.8}$$

2.4 Soliton microcombs

Microcombs are optical devices that generate several evenly spaced and phase coherent optical frequencies from a single one [1]. This looks like a comb in the frequency domain, as seen in Figure 2.3. This corresponds to a train of pulses in the time domain as seen in Figure 2.3 as all lines are in phase. This pulse, a pulse that stably propagates through a dispersive medium without changing shape, is called a soliton [1].

The structured output of a comb in a microresonator is a result of a balance between four effects. On one hand Kerr nonlinearity is balanced against dispersion. And on the other hand losses, both intrinsic losses in the waveguide as well as extrinsic losses at the output port, are balanced against the input power into the resonator. The phenomenon is explained mathematically with the dampened and driven nonlinear Schrödinger equation [19].

The output spectrum of an ideal comb is given by narrow lines at the frequencies specified by Equation 2.9 [1, 5], where k is an integer number, known as the mode number, and f_0, f_r are the offset frequency and repetition rate respectively.

$$f_n = f_0 + kf_r \tag{2.9}$$

The pulses seen in Figure 2.4 shows how Equation 2.9 relates to the time domain. The pulses are separated by a time $1/f_r$ and the additional phase between carrier and envelope is related to the offset frequency f_0 [3].

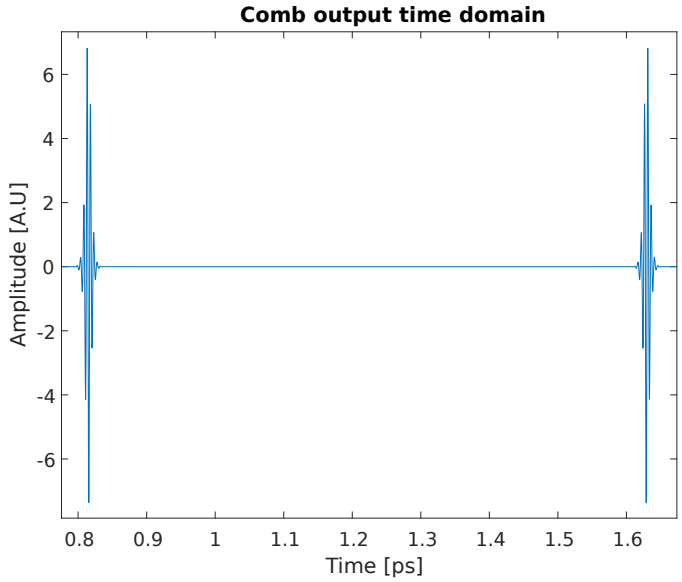

Figure 2.4: Two pulses from the comb in Figure 2.3. Notice the phase shift between the carrier and envelope waves that appear between cycles. The first pulse has one peak after the main peaks whereas the second pulse has one peak before the main peak. The pulse-like nature of the comb stems from the fact that the generated optical frequencies are all phase coherent.

Photonic molecule microcombs operate with the same principles as the microcombs. However, the wide soliton existence regime [22] and additional degree of freedom, two heaters instead of one, enable simpler operation practically.

2.5 Soliton in photonic molecule

To create a soliton in a photonic molecule microcomb, two things must happen. The mode of the resonators must first be aligned by shifting the uncoupled resonant frequency of one or both of the cavities to the same frequency [22]. The shift is realized by altering the temperature of the resonators using on-chip microheaters as the mode depends on β (Equation 2.5). The thermo-optic effect changes n, and thus β, as T changes. The second step is to align the pump laser frequency with a longitudinal mode of the coupled cavities which begins building up power inside the cavity.

The buildup of power inside the cavity enables nonlinear effects inside the cavity and which create new frequencies by a process called Four Wave Mixing (FWM) [19, 18]. FWM consumes two photons of equal frequency (and thus energy) and produces two new photons while conserving energy and momentum of the photons [3, 18]. The conservation of energy causes the two generated photons to be equidistant from the pump frequency ($E = \hbar\omega$) which means that sidebands are generated symmetrically. The new frequency circulates inside the cavity and if it aligns with a longitudinal mode and the amount of converted power is sufficient to overcome intrinsic and extrinsic cavity losses the nonlinear effects repeat at the new frequency. This process

of FWM and buildup at the longitudinal modes of the cavity repeats until a comb is formed.

2.6 Noise in microcombs

The noise of a microcomb depends heavily on its formation [24, 19]. A low noise comb is achieved in two ways. It is either formed into a low noise state or evolves into one. A low noise state is achieved when dispersion and cavity decay rate are equal and the detuning is small [24]. The cavity decay rate is increased by both intrinsic losses as well as power leaving the resonator to be used in applications. Both these parameters are somewhat tunable during design [35] and manufacturing of the comb.

In the context of comb generation, a low noise comb is formed when the initial FWM process generates new lines separated from the pump by exactly one FSR. However, depending on the cavity itself other non integer multiples of the FSR could be generated instead [24] which constitutes the noisy state.

The dominant source of noise in Si_3N_4 microcombs is the thermo-refractive noise [36] which acts in the kHz to MHz range [37]. This noise stems from thermal fluctuations in the cavity that alter its resonant frequency through thermo-optic and thermo-elastic effects [33], thus changing the detuning which affects the comb repetition rate and offset frequency through Raman self-frequency shift [**?**, 38]. Other noise sources such as shot- and quantum noise also affect microcombs but are of lower magnitude and much more broadband.

The relation between detuning and repetition rate is nonlinear and contains a flat region [39]. This is because the relation between repetition rate and detuning is influenced by both Raman frequency shift [38] and soliton recoil [39]. This means that there exists a point in the δ, f_r relation around which a small variation in detuning has a minimal impact on the repetition rate. This point is called the quiet point and the microcomb should be operated at this detuning to minimize both phase noise and drift.

2.7 Soliton power in microcomb

A soliton propagating in a microresonator is characterized by a detuning dependent power as described by Equation 2.10 [27, 29], where A_{eff} is the size effective area of the propagating optical mode and $\eta = Q/Q_{external}$, Q the loaded quality factor, n_2 the Kerr nonlinearity coefficient and δ the detuning. This means that a constant detuning can be achieved if one locks the output power level to a fixed point. This results in compensation of variations in β_1 from thermo-optic noise. Such a system has been demonstrated in [28] for single resonator microcombs.

$$P_{sol} = \frac{2\eta A_{eff}}{n_2 Q}\sqrt{-2nc\beta_2\delta} \tag{2.10}$$

Equation 2.10 only holds when one or more solitons propagate in the comb [29]. Other comb states that appear while initiating a soliton microcomb show no analytical relation between detuning and power. These states must be avoided for operation of the control system. This limitation is not an issue during operation as the soliton state is desired for operation. However, the limitation makes the controller unusable during initiation as other states appear before a soliton forms.

2.8 Photodiodes, mixing and beating

Photodiodes (PDs) are essential for measuring photonic systems. Since they allow the optical domain to be viewed by instruments that respond to electric signals. A PD produces an electrical current proportional to the incoming optical power as shown in Equation 2.11.

$$I = \alpha P_o = \alpha |e|^2 \tag{2.11}$$

A photodiode converts the incoming optical power to a current. This intrinsic nonlinearity means that they act as mixers. Consider two optical signals $e_1 = a_1 \sin \omega_1 t$ and $e_2 = a_2 \sin \omega_2 t$ both interacting with a photodiode. This gives a current as follows.

$$I = \alpha(e_1 + e_2)^2 = \alpha(a_1^2 \sin \omega_1 t^2 + a_2^2 \sin \omega_2 t^2 + 2a_1 a_2 \sin \omega_1 t \sin \omega_2 t) \tag{2.12}$$

Equation 2.12 can be compared to a traditional microwave mixer. The $\sin^2$ terms will generate power at 0 Hz and $2\omega_i$ whereas the third term will generate power at $\omega_1 - \omega_2$ and $\omega_1 + \omega_2$. Since ω_i is above the bandwidth of electronics (about 200 THz), only the 0 Hz and $\omega_1 - \omega_2$ components of the signal will be visible after the PD.

The method described above of combining two optical signals, mixing them with a photodiode and removing the high frequency components is called beating. It is a technique commonly used for photonic measurements.

2.9 Fiber to chip interface

Classical optical equipment is interfaced with optical fibers. However, the chips capable of generating frequency combs are not interfaced with fibers. They instead have tapered couplers placed at their edges which allow a lensed fiber to couple light into or out of the chip. This setup is visualized in Figure 2.5 as seen from above. The coupling between fiber and chip is as good as possible when the optical mode propagating inside the fiber overlaps with a mode that is allowed to propagate inside of the waveguide.

Losses of 2 dB to 3 dB are expected at each coupling interface. As seen in Figure 2.1, the mode inside of a waveguide is about the size as the waveguide itself. This means that achieving a perfect overlap requires sub-µm positioning accuracy, precision and stability.

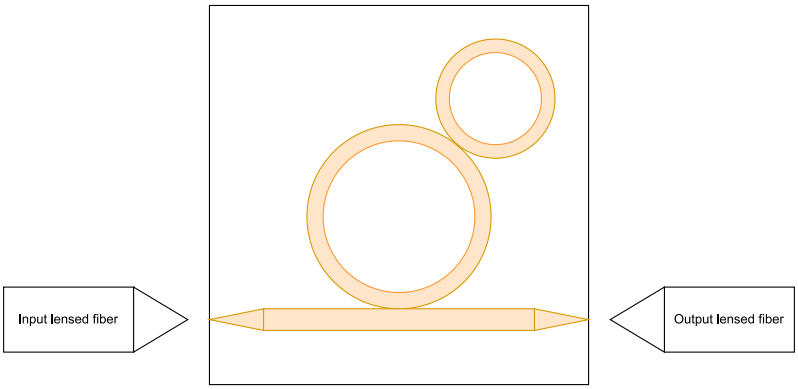

Figure 2.5: Two lensed fibers couples light into and out off the chip containing the photonic molecule. Misalignment of these fibers result in optical losses.

Fine adjustment for the coupling stages is achieved by piezoelectric controllers which extend and retract the fibers by an applied voltage [40]. These stages are capable of positioning the fibers within 200 nm. However, they can not keep this position for an extended duration as thermal expansion and human interaction move the fibers. This results in additional losses to the input and output of the comb. The input power is essential for the existence of a comb [22]; if the drift is too large the comb could be destroyed.

The proposed comb stabilization method relies on locking the detuning dependent soliton power to a constant. If the output coupler in Figure 2.5 moves the measured comb power would be affected by the additional loss. This causes the controller to lock the comb to another detuning, introducing additional noise and drift. This adds an extra term to the converted power measured off chip, Equation 2.13, where α represents the coupling loss and P_{sol} the soliton power from Equation 2.10.

$$P_{sol,out} = \alpha P_{sol}(\delta) \tag{2.13}$$

The system is less sensitive to drift of the input coupler. The existence regime for photonic molecule microcomb is quite large [22] both in terms of detuning and input power. The Raman shift is also independent of input power [**?**] which means that variations in input coupler loss do not correspond to variations in repetition rate.

2.10 Control theory

This thesis deals with controlling a frequency comb therefore basic concepts within control theory are useful for understanding the methods and results.

Figure 2.6 shows a typical controlled system. The linear system F is controlled by negative feedback and the linear controller C. Its transfer function is given by Equation 2.14 for a traditional PID controller.

$$U/E = K_p + \frac{K_i}{s} + K_d s \tag{2.14}$$

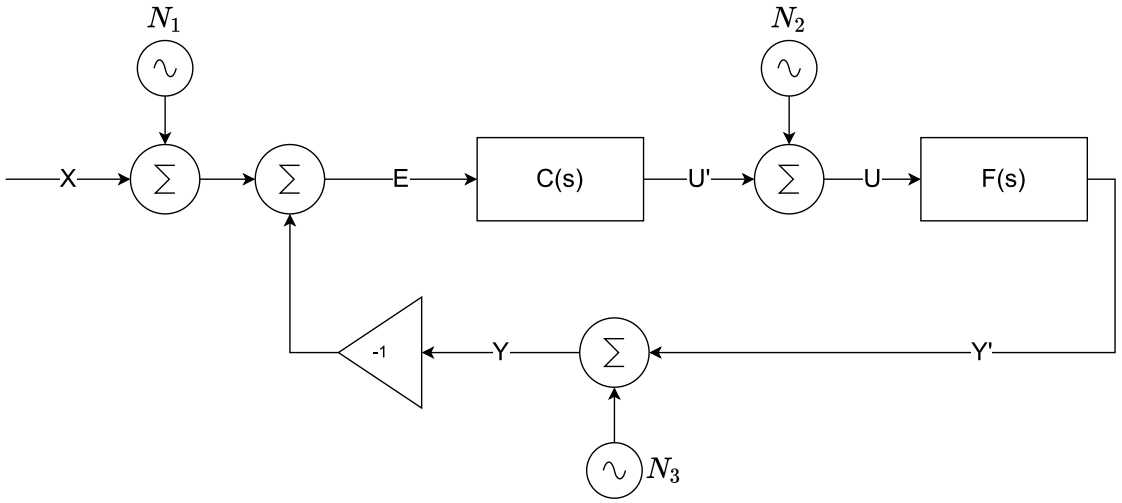

Figure 2.6: A controlled system with input X and output Y. Noise sources N_i represent noise added at different locations in the system. The controller C controls the input of the uncontrolled system F such that the error signal E is kept at zero. N_2 represents noise coupled onto the control signal. This noise has a large impact on the state of the system as it is coupled straight into the input of the system F. Noise from the input signal, N_1, as well as noise from the feedback loop, N_3 can be attenuated by the controller and is of lesser importance. Section 3.5.4 relates the noise sources shown in this figure to the physical system.

Figure 2.6 also shows noise sources. Noise from N_2 has the largest effect on the system as the controller is unable to compensate for that noise before it influences F and thus the output Y. The two other noise sources N_1 and N_3 are compensated for within the bandwidth of the controller C.

The terms of the PID controller determine the stability and speed of the controller. A higher proportional gain K_p gives a faster but less stable, and therefor more prone to overshoot and oscillations, controller. A larger K_i gives a better compensation for low frequency errors and a smaller residual error in steady state, it also degrades stability. The K_d term on the other hand increases the stability margins making the system more stable but increases the influence of noise on the system. In general K_p, K_i should be as large as possible to avoid oscillations, whereas K_d should be set to keep output noise low and enable an increase of K_p and K_i.

3

Methods

This chapter explains the system used to control the photonic molecule microcomb as well as the methods used to evaluate the performance of the comb and control system combined.

3.1 Repetition rate measurement

One important parameter of the controller is its noise performance. The amount of noise that is added or removed by actively controlling the comb is of interest if the controller is to be used for any noise sensitive measurement. This is the performance metric of the controller. These measurements are to be performed out of loop on both a controlled comb and a free running comb in order to isolate the impact of the controller.

The simplest measurement of the comb repetition rate is to connect a PD and frequency counter of sufficient bandwidth to the output of the comb. The photodiode will produce a pulse for each incoming pulse of light which is counted by the counter. This is unfeasible, but not impossible, since the repetition rate f_r of the utilized combs is about 50 GHz and the fastest currently available photodiodes reach about 50 GHz [41]. However, smaller resonators with even larger FSR can not be measured directly. Thus, an indirect method has to be used.

Such a method modulates a part of the comb with an RF tone. Assuming that this modulation is strong enough to show nonlinear effects in the modulator, the spectrum in Figure 3.1 is achieved [42]. Beating this spectrum on a photodiode with a bandwidth below that of the modulation oscillator gives a single low frequency tone f_m which is related to f_r according to Equation 3.1 [42], where n is an integer indicating how many higher order sidebands has been generated by the nonlinear modulator. The method is called Optoelectric Downconversion and its setup is visualized in Figure 3.2.

$$f_r = n f_{eom} \pm f_m \tag{3.1}$$

A disadvantage of this method is that changes in the reference frequency f_{eom} are multiplied by n before influencing the measurement. This limits the smallest measurable drift and phase noise using the method. This also amplifies phase noise from the reference to the measured repetition rate. This method also introduces a

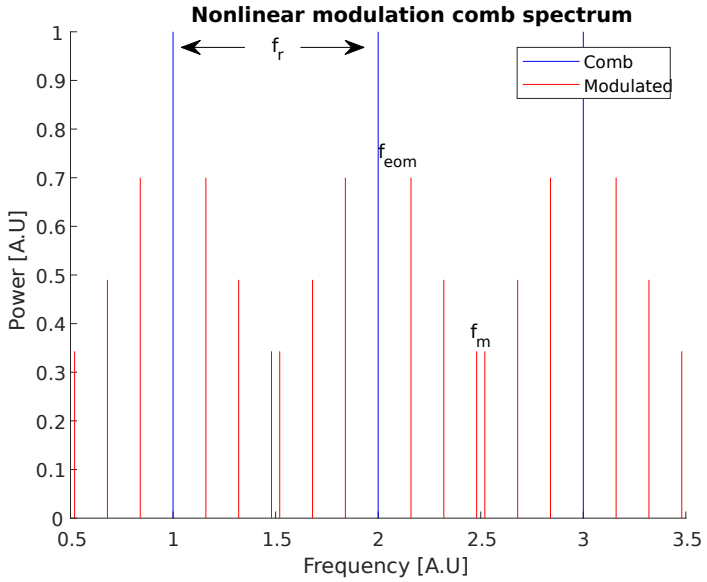

Figure 3.1: Effect of nonlinear modulation on comb output. The frequency f_m is sufficiently low to be counted by conventional electronics. Case when $n = 6$ and the repetition rate is larger than nf_{eom} in Equation 3.1

large loss of power because of the high insertion loss of the modulator. This limits the optical signal to noise ratio that is achievable, thus setting a limit for noise measurements.

Another disadvantage with the method is that the absolute value of the repetition rate requires multiple measurements with different f_{eom}. However, as the purpose of this measurement is to track changes in repetition rate and not the absolute values, the method is suitable.

3.2 Locking the pump laser frequency

A stable pump laser is essential, since it affects the offset frequency of the comb [19]. A phase locked loop achieves this using a tunable laser and a fixed laser if a beat note between the two can be observed in the microwave domain [1]. A commercially available octave spanning frequency comb [17] locked to a microwave Global Positioning System (GPS) source is used as a reference.

The low repetition rate of the commercial comb creates beat notes within the RF domain which are locked to a microwave signal that is in turn locked to the reference clocks in the GPS satellites giving any laser traceability to the definition of time. Figure 3.3 illustrates the lock, the part surrounded by dotted lines is available as a commercial system from [17].

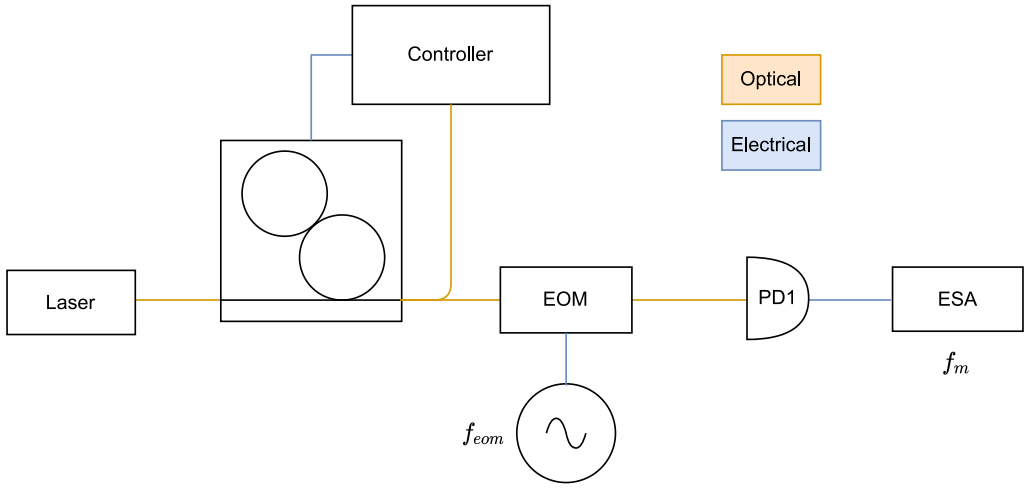

Figure 3.2: Repetition rate measurement setup [42] using Optoelectric Downconversion (OEDC). Shows out of loop measurement of f_r using Equation 3.1 and the nonlinear modulation shown in Figure 3.1. The ESA can also be used to measure the phase noise of the repetition rate. However, it will also be influenced by the phase noise of the reference oscillator. Electro-Optic Modulator (EOM), Electrical Spectrum Analyser (ESA)

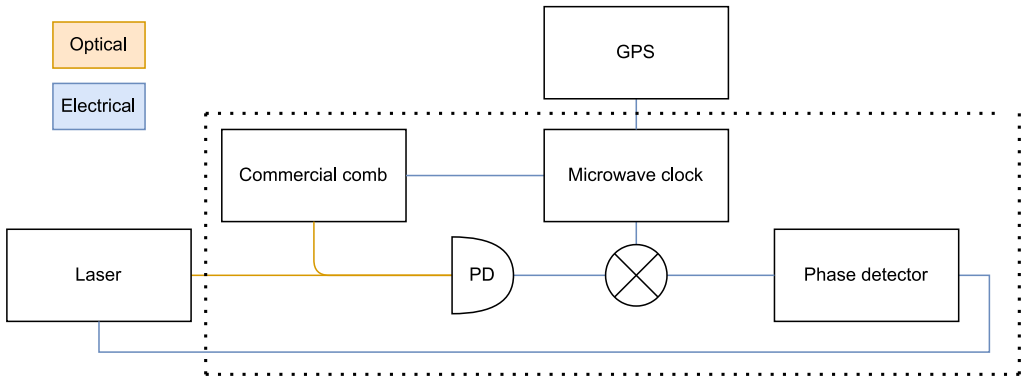

Figure 3.3: Block diagram of method to lock any controllable laser to an external GPS reference. The dotted lines correspond to the commercial system [17]. Global Positioning System (GPS), Photodiode (PD)

3.3 Measuring the response time of the heater

The heater power is the primary control signal by which the comb is stabilized. This is because it is able to control the pump resonance detuning, by changing the resonant frequency of the system. In order to compensate for the thermo-optic of the first order noise of the comb, the control loop should be able to operate around the 1 MHz range. It is therefore of interest to measure how quickly the heater is able to thermo-optically control the comb.

The resonator should be pumped at low power to minimize the impact of thermal instability [33]. The low power condition is verified by fitting a Lorentzian, L, (Equation 3.2) as the thermally unstable state is characterized by a triangular resonance [33]. The laser frequency is swept across resonance and the transmission spectrum is recorded. This is then fit to Equation 3.2 where a_i are fit parameters and ω optical frequency.

$$L = a_0 + \frac{a_1}{1 + (\frac{\omega - \omega_0}{\omega_{fwhm}})^2} \tag{3.2}$$

The weakly pumped resonance is then subject to steps in heater power. These steps result in a change of refractive index and thus a change in resonance frequency which translates to a change in output power from the resonator. The measured power should increase as the heater moves the longitudinal mode closer to the pump frequency and decrease vise versa. An exponential function (Equation 3.3) is fit to both rising and falling edges of the step to calculate the time constant of both heating and cooling on both sides of resonance. This method assumes that the response from heater power to transmission is linear. The response is a nonlinear Lorentzian, and therefore nonlinear effects are expected. However, a Lorentzian can be approximated by a linear equation for $|t - a_2| \lessapprox a_3$ and $sign(t - a_2)$ constant.

$$T = T_\infty - (T_\infty - T_0) \exp(-t/\tau) \tag{3.3}$$

The left half of Figure 3.5 shows the transmission of the resonator as the wavelength of the input laser is swept linearly. Equation 3.2 is successfully fit to the data meaning that the resonator is pumped at sufficiently low power to avoid thermal nonlinearity and instability.

One input and output combination of the weakly pumped resonator is shown in the right half of Figure 3.5. It shows the exponential increase and decrease from which the time constants were extracted by fit of Equation 3.3.

Figure 3.6 show response times for different step sizes. A nonlinear behavior, a changing time constant with input amplitude, is seen. This is expected as the transfer function from detuning to transmitted power is proportional to $1/\delta^2$. Heating also appears faster than cooling which is expected as the heating element, the heaters, have higher thermal coupling to the resonator than the cooling element, conduction to ambient. This could be resolved by using a Peltier element, which is capable of both heating and cooling, for thermal control. pro The response times are

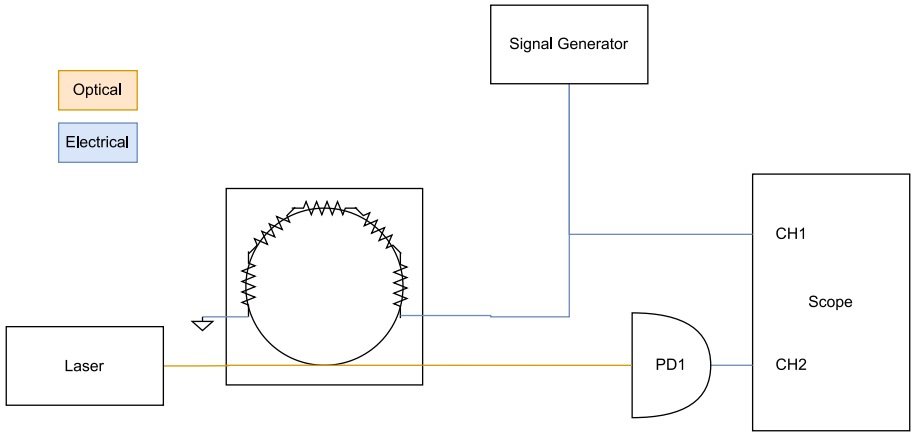

Figure 3.4: Measurement setup for heater response time measurement. A laser weakly pumps the resonator slightly off resonance while the transmission is monitored by a photodiode and oscilloscope. The signal generator applies a step function to the heater which shifts the resonance frequency of the resonator. The event is captured by the oscilloscope and fetched for post processing.

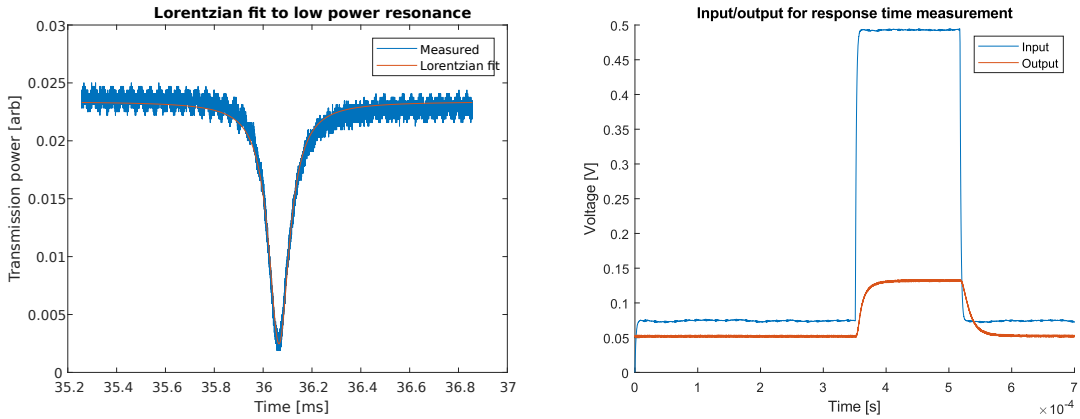

Figure 3.5: Left: Transmission as a function of time as the wavelength of the pump laser is swept linearly. A Lorentzian function (Equation 3.2) is fit to the data to show that the resonator is weakly pumped. Right: Input to the heater and output of resonator when the resonator was pumped from the red side.

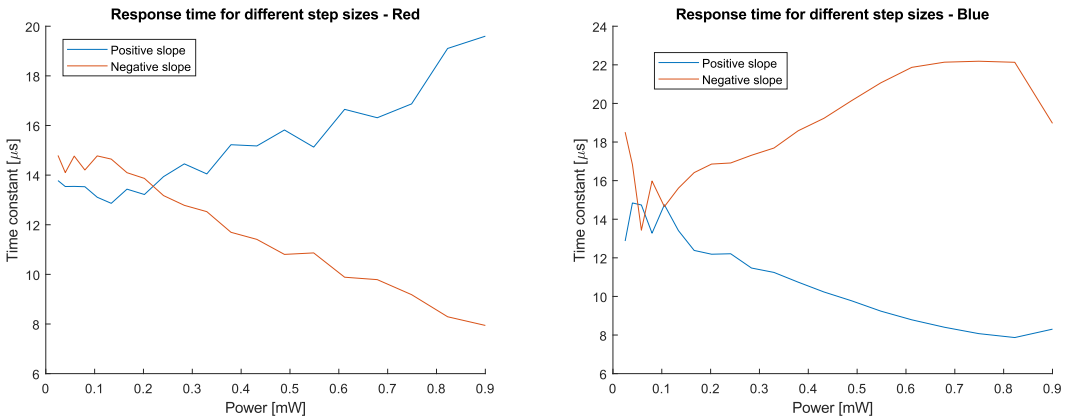

Figure 3.6: Resonator transmitted power response time when excited by a power step at the resonator's heater. The left figure shows the red detuned case, where the pump laser is placed red, at a larger wavelength, of the resonance. The right figure shows the blue detuned case. Notice that the figures are quite similar meaning that nonlinear thermal effects of a microresonator are dampened in the experiment.

similar for both sides of the resonance which is expected as the Lorentzian resonance is symmetrical around the longitudinal mode for low pump power. The response time varies between 8 µs to 22 µs. Therefore, a maximum control loop bandwidth of about 100 kHz can be used with the integrated heaters. [43] also uses heaters for thermal control of combs and estimates the time constant of the thermal events around 10 kHz.

3.4 Photonic molecule microcomb initiation

The physical initiation of a photonic molecule is explained in Section 2.5. However, how this is done in practice influences the design of the control system as well as an automated initiation system.

First, an operating point should be located. The operating point is the laser frequency in combination with the applied electrical power to both heaters. An operating point supporting comb generation is found by sweeping the laser frequency across the FSR of the cavity with largest FSR and moving the resonances to a split using the heaters. A good operating point is identified by an increase in converted power as the laser sweeps across the resonances. The laser can then be tuned past the first and towardscharacterised the second resonance until a frequency comb is created.

Second, the comb is tweaked to a soliton state such that Equation 2.10, which enables active control through converted power, holds. This is achieved by fine adjustment of the heater powers to change the detuning. The heater operating point is usually in the order of several V and the comb state is tuned to a soliton by 10 mV or 1 mV adjustments. A single soliton comb state is characterized by a flat or linearly decreasing power spectrum as well as a repetition rate as set by the geometry. Both the optical spectrum and the down-converted repetition rate, as explained in Section

3.1, are monitored to find a suitable comb state.

The controller is then activated. However, if a large voltage step, multiple 10 mV, is applied to the heaters the comb will be pushed beyond the previously found operating point and collapse. The state of the controller must be reset and its output set close to the middle of its range before activation. The converted power set point must also be selected to the current state of the comb to avoid large output steps. Operation in the quiet point is beneficial for comb stability as discussed previously. The quiet point is found by changing the set point of the PID controller and monitoring the output spectrum for a local minimum. This works because the soliton power is characterized by a specific detuning and detuning is related to soliton power via Equation 2.10.

3.5 Control system

The control system is visualized in Figure 3.7. It shows the control system with both in and out of loop measurements as well as the equipment needed to find the operating point of the photonic molecule. The signal generator is used to tune the operating point of the heaters to allow for comb generation.

The control loop consists of a narrow and sharp band pass filter that picks one or two comb lines to use for measuring the converted power. Few lines are used in order to avoid the controller believing that redistributing the comb power is stable. This power is detected and a set amount, the set point, is subtracted off to create an input signal for the PID controller. It alters the primary heater power in order to keep the converted power stable. The input signal to the controller is monitored externally to understand how well the used PID parameters stabilize the converted power.

Two measurements are taken out of loop. One is the total power measured which is dominated by the laser power that gets transmitted through the resonator. The other is the electrical spectrum around the opto-electrically down-converted repetition rate of the comb. Both of these measurements should be constant if the controller manages to overcome environmental changes and stabilize the comb.

3.5.1 FPGA and processing system

The Red Pitaya (RP) combines an Xilinx system on chip featuring programmable logic and a hard ARM processor with two 14 bit ADCs and DACs [31]. All four converters of the RP operate at 125 $\mathrm{MS\,s^{-1}}$ with an analog bandwidth of 60 MHz.

The processing capabilities of the RPs programmable logic enables real-time signal processing applications where as the processing system provides a familiar environment for development of user interfaces. The project is available as an open-source software but closed-source hardware product which invites contributions from the community [31].

One such contribution from the community combines a PID controller with a waveform viewer [44]. Its user interface allows for configuration of PID parameters and

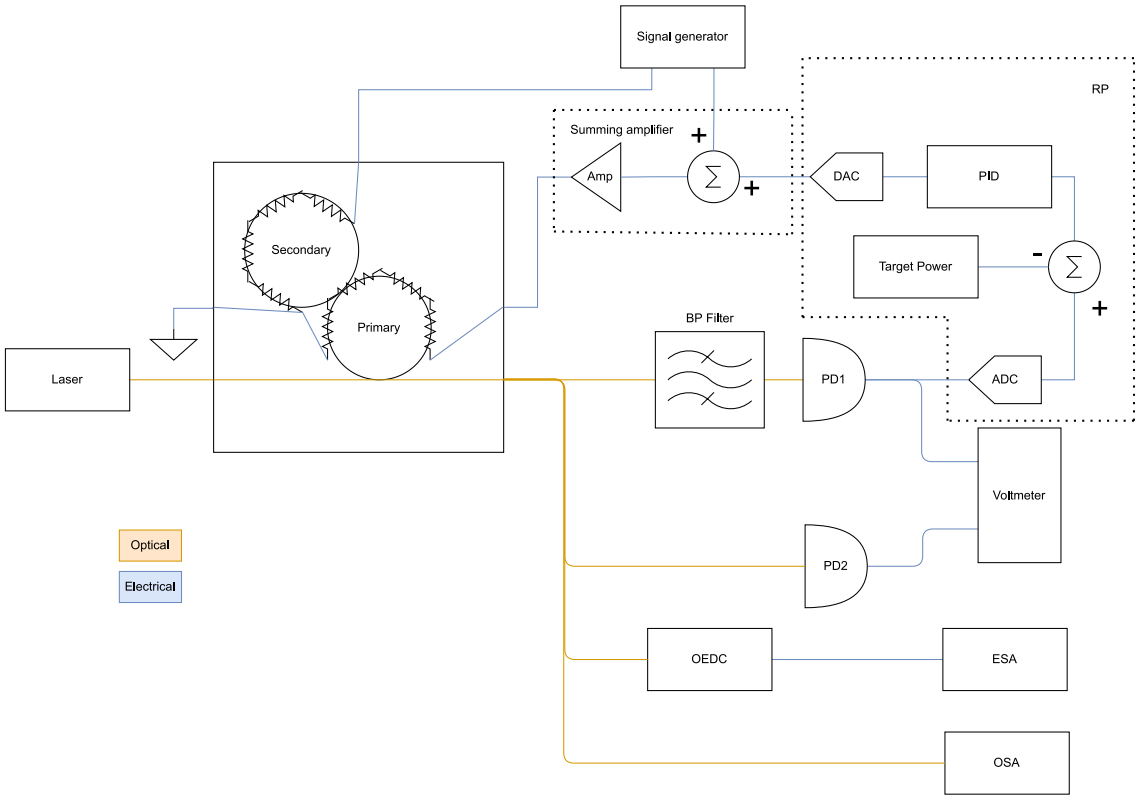

Figure 3.7: System overview for stabilizing a photonic molecule microresonator. The primary heater is controlled by a PID controller using a set point in converted power as an error signal. The optical filter selects a few lines to be used as a measure of the converted power. The performance of the controller is measured both in loop with PD1 and the voltmeter as well as out of loop with OEDC. Optoelectric Down-conversion (OEDC), Electrical Spectrum Analyser (ESA), Proportional-Integral-Derivative (PID), Photodiode (PD), Analogue to Digital Converter (ADC), Digital to Analogue Converter (DAC), Optical Spectrum Analyser (OSA), Red Pitaya (RP).

offset for the error signal as well as enabling, disabling and resetting the regulator all while observing the input and output of the system in real time. This flexibility is especially useful since the manual frequency comb initiation sequence is quite involved.

3.5.2 Signal converters

The DAC is located between the controller and the system, N_2 from Figure 2.6, and thus its noise performance is essential for the noise performance of the control loop. A converter with a large resolution or a converter with a large bandwidth followed by a low-pass filter at the maximum loop bandwidth should be used to reduce both quantization noise and uncorrelated random noise on the control signal.

The ADC quantizes the response of the system before the PID controller. The noise added by the converter is an input to the controller and can be compensated for by the control loop. A higher resolution and or lower noise converter is beneficial but not as critical as the DAC that controls the comb.

3.5.3 Amplifier

The integrated heaters require some power to be driven. Their resistance varies within $50\,\Omega$ to $500\,\Omega$ and are able to operate with voltages up to $5\,\mathrm{V}$ to $10\,\mathrm{V}$ before breaking. The lower the resistance the lower the maximum operating voltage. This means that up to $0.5\,\mathrm{W}$ is needed to utilize the full dynamic range of the heater. The DACs inside the RP are able to output their full range into a $50\,\Omega$ load. However, their full range is only $\pm 1\,\mathrm{V}$. A power amplifier is therefore needed to control the heaters with the RP.

The operational point of the system must be found prior to enabling the controller. This requires adjustment of heater voltage which then should be combined with the controller output. A summing amplifier accomplishes this as shown in Figure 3.7. The amplifier is coupled to the input of the photonic molecule and noise contributions from the amplifier are reflected in the output before compensation by the control system. This means that a low noise amplifier with a sufficient power rating should be used.

3.5.4 Noise sources

Figure 2.6 shows three noise sources N_1, N_2, N_3 which all correspond to some physical phenomena in the designed system. N_1 is noise in the set point, this would be caused by the digitization of the set point. As the set point is constant during operation the system is not influenced by this noise. However, the dynamic range of which values of detuning the system can be locked to is determined by the resolution of the set point.

N_2 represents noise between the controller and the comb. This includes quantization noise in the DAC, electronic noise from the summing power amplifier and any signal picked up by the connection between amplifier and comb.

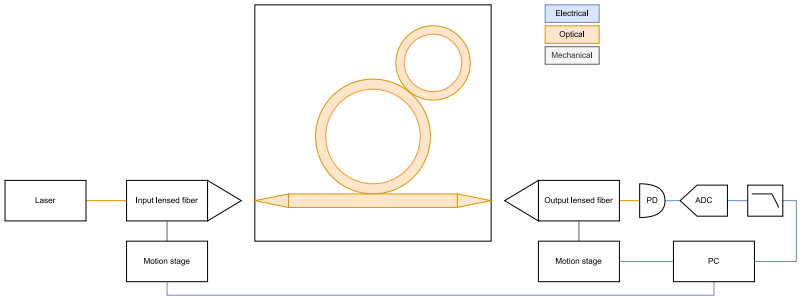

Figure 3.8: Setup for minimizing the losses through the coupling stage by actively moving the lensed fibers. The transmitted optical power is measured and the motion stages acted on via serial commands to maximize the optical power. A low pass filter removes interference from the comb stabilizing controller. Personal Computer (PC), Analogue to Digital Converter (ADC), Photodiode (PD).

N_3 includes the thermo-refractive noise from the comb, shot noise and electronic noise from the PD that converts the optical power to a voltage, as well as quantization noise in the ADC.

3.6 Compensating for drift of coupling

The input and output lensed fibers need to supply the comb with a constant power to keep the soliton state [22] as well as keep the output loss constant as to not change the measured converted power when the detuning is constant. This requires a stable coupling. One method to achieve that is to package the chips, which eliminates the need for coupling stages altogether. This can be done by fusing a fiber onto the edge of the chip [45]. However the available chips do not have this capability and another method must be used.

One such method is to actively try to maximize the transmission power. This is achieved by measuring the transmission, moving one axis of the stage, measuring again and picking the position with highest transmission power. This procedure is continuously repeated for all six axes of the input and output stages to keep the power at the highest possible value. Figure 3.8 shows the feedback loop from transmitted power to stages. The PC runs the algorithm as described above. The real time performance of a desktop PC is limited but sufficient in this case as actions can only be taken every couple of 100 ms as the mechanical movement of the stage is slow.

As the transmitted power depends on detuning and the comb is stabilized by controlling detuning, there is a possibility for interference between the coupling controller and the comb controller. The two controllers are decoupled from each other by inserting a sharp digital low pass filter in the signal path of the coupling stabilizer as indicated in Figure 3.8.

This control scheme was evaluated while pumping the resonator off resonance and thus not generating a comb in order to avoid any interaction between the two control loops.

4

Results

This chapter presents the performance, with respect to stability and phase noise, evaluation of the control system acting on a photonic molecule frequency comb. It also investigates two sources of errors and outlines a fix to one of them.

4.1 Repetition rate long-term stability

The down-converted spectrum of the comb repetition rate was monitored for an extended duration with and without the PID controller enabled. Figure 4.1 shows the evolution of the spectrum for both cases. The controlled case shows an increased stability with lower frequency drift compared to the uncontrolled case. The reduced drift is also seen in the converted power measurement where the converted power is fixed when the controller is enabled and not fixed when it is uncontrolled. This comparison is shown in the lower left part of Figure 4.1. A down converted repetition rate peak to peak drift of 5 kHz during a time interval of 20 min is achieved for a nominally 50 GHz f_r photonic molecule when the controller is active. In contrast, the repetition rate of the uncontrolled comb drifts by 25 kHz during a similar time frame.

The repetition rate drift is correlated to the change in transmitted power which is seen in the lower right of Figure 4.1. The observed drift in transmission power corresponds to about 0.2 dB peak to peak. Both transmitted power and repetition rate are related to the detuning of the comb; the transmission power by Equation 2.4 and the repetition rate via Raman soliton self frequency shift [**?**, 38]. The detuning is also related to the converted power via Equation 2.10. However, losses in the output coupler would introduce an additional, time dependent loss to the system that is not accounted for in Equation 2.10. This loss causes the converted power set point which the controller locks to to correspond to a different converted power on chip. Different converted powers on chip could explain how the detuning changes while the measured converted power does not.

The observed change in detuning could also be explained by Equation 2.10 as it contains an n. The photonic molecule microcomb is controlled by change its temperature which in turn will influence n. A change in n is used to control δ to stabilize the comb. However, the n found in Equation 2.10 means that the soliton power can remain constant even when the detuning is changing as long as the temperature is changing as well. This dependency could be the cause of some of the observed drift when the controller is active.

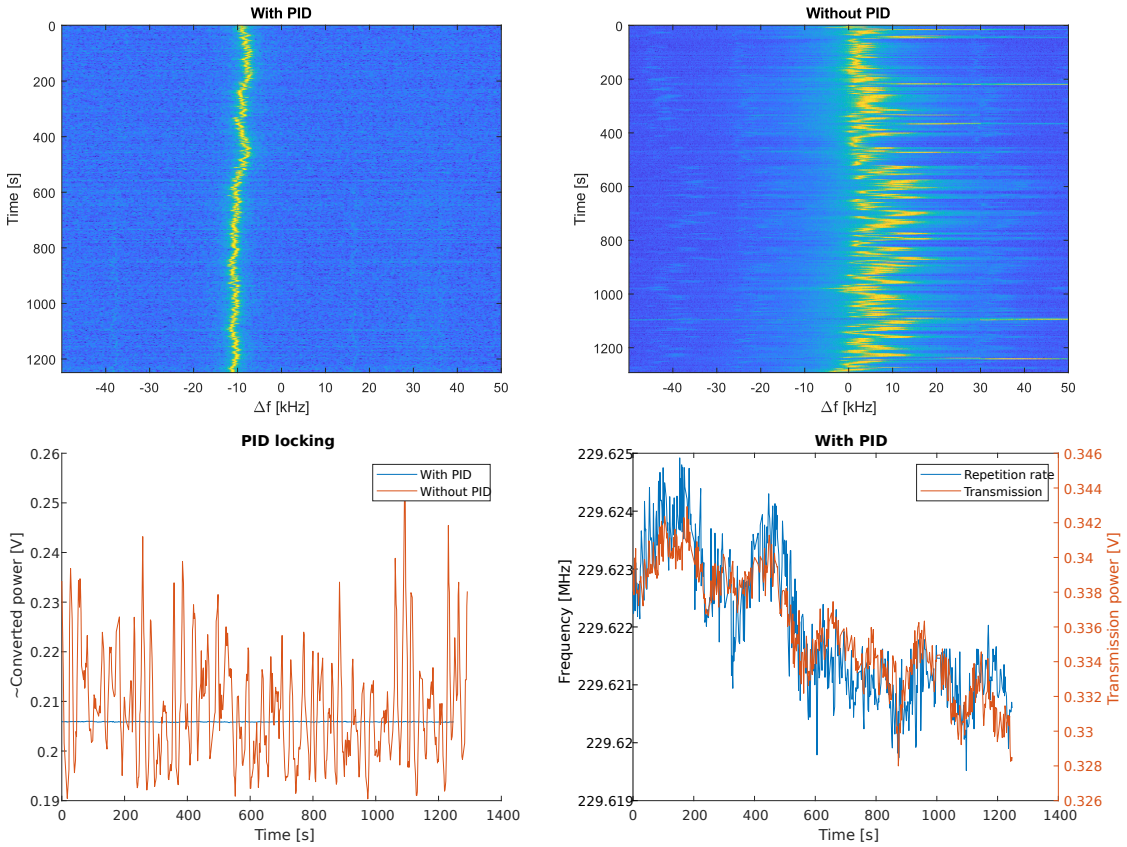

Figure 4.1: Stability of repetition rate with and without the PID controller enabled. Top left figure shows a controlled comb whereas the top right shows a free running one. A more yellow color corresponds to a higher power level. Spectrum is sampled with a resolution bandwidth of 100 Hz. The bottom left figure shows the converted power which is locked to a fixed value for the controlled comb and influenced by ambient effect for the uncontrolled comb. The bottom right shows how the power of the pump laser transmitted through the resonator correlates with the repetition rate for a controlled comb.

4.2 Impact of optical filter

The impact of the bandwidth of the converted power optical filter (location given in Figure 3.7) was investigated. Figure 4.2 shows the relationship between converted power and repetition rate for an optical filter bandwidth of one and four comb lines. The controller is configured identically for both measurements to enable comparison. However, the narrow filter allows for a wider range of stable PID parameters. The systems can be considered comparable, apart from the different optical bandwidth, as both measurements feature a repetition rate minimum around 218.99 MHz and the minima occur at a similar converted power per line. The difference in converted power per line at the minimum repetition rate can be attributed to an offset error in the RPs ADC.

The variation in repetition rate around one converted power corresponds to a short term measurement of drift. The narrower filter contains about half of the drift compared to the wider filter when comparing around the quietest point which is located slightly right of the minimum repetition rate.

The shape of the graphs in Figure 4.2 is also interesting. Both filter bandwidths show a second order relation with one noisy side, towards lower converted power, and one less noisy side. The point with lowest the frequency noise is located at slightly higher converted power than the local minima in repetition rate. This provides insight for how one would lock the repetition rate optimally to a frequency reference using a phase locked loop.

4.3 Repetition rate phase noise

Figure 4.3 shows the measured phase noise of the down-converted repetition rate of a comb. The comb is not generated by the same chip as the combs from Figure 4.1 as that chip was destroyed. The stability of this device is slightly worse than the device shown in Figure 4.1.

The left part of Figure 4.3 shows the phase noise when the input laser is locked to a GPS reference and the right figure when the input laser is free running. Notice that locking the input laser has about the same impact as locking the detuning with the heaters. The lowest phase noise is achieved when both locks are used at the same time.

Figure 4.4 shows phase noise measurements with different PID controller settings. The K_i component of the controller was changed between measurements while keeping K_p constant. An increase in phase noise of the controlled case in relation to the uncontrolled case is seen for offset frequencies larger than K_i. This confirms that the frequency range within which the controller is able to compensate for phase noise is related to the integrating bandwidth of the controller.

The controlled phase noise with the locked input laser is degraded slightly at large offset frequencies as seen in the right plot of Figure 4.3. This degradation is caused by the controller as its integrating bandwidth is limited to about 5 kHz for stability. The bandwidth of the heater is larger than that and excess signals generated by

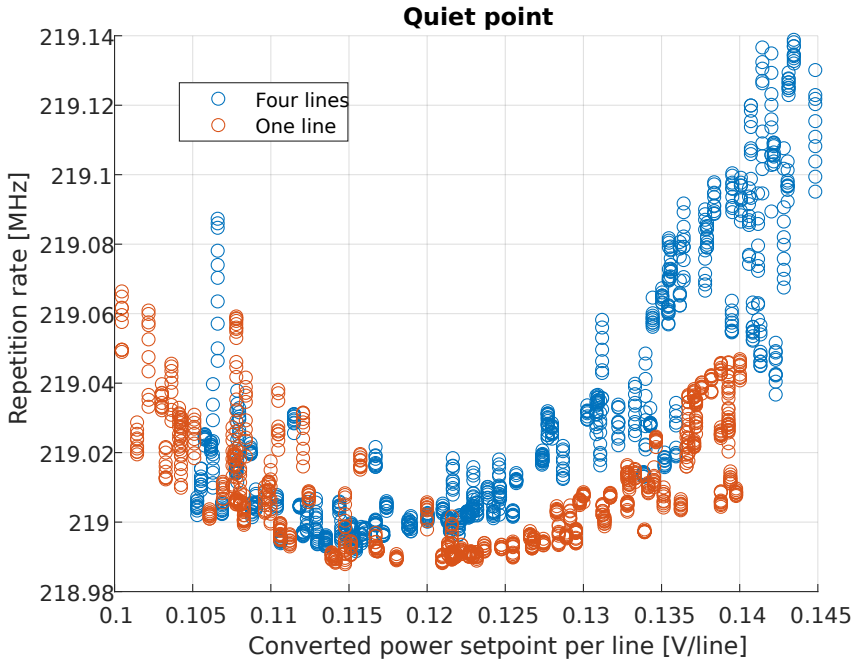

Figure 4.2: Measured repetition rate as a function of converted power set point. Multiple measurements have been performed on the same set point to get a sense of the noise at that lock. A second order relation between converted power and repetition rate is seen.

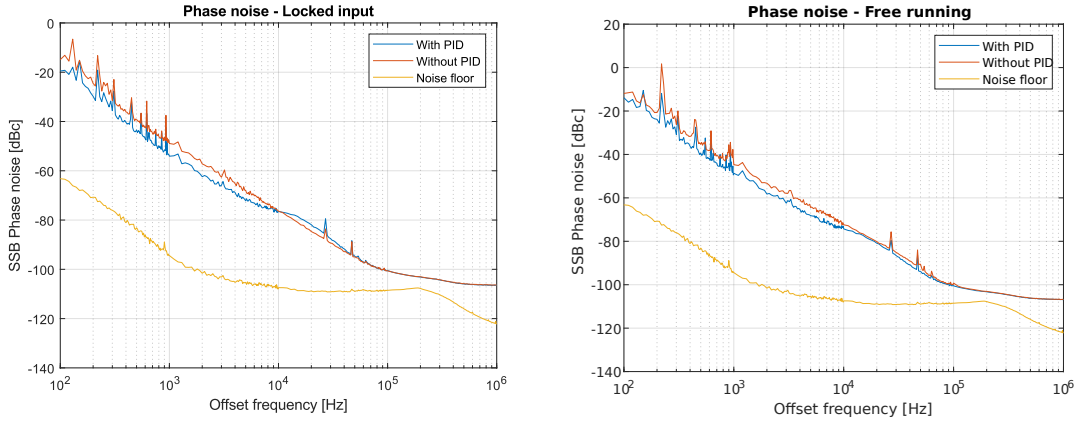

Figure 4.3: Single side-band phase noise of down converted repetition rate (using OEDC) for a controlled and uncontrolled comb. The input pump laser is locked to a GPS via a commercially available frequency comb [17] in the left figure and not in the right one. Both figures show the noise floor as given by the reference oscillator used for OEDC.

the controller influences the comb. We predict that this noise can be attenuated by increasing the integrating bandwidth of the controller.

The top and bottom left part of Figure 4.4 show two cases of instability. The phase noise is seen to increase locally around 1 kHz and 8 kHz respectively. These peaks correspond to oscillations in the controller output around those frequencies indicating an improperly tuned controller. These oscillations can and should be removed by changing K_i, K_p or P_{sol}. However, this was not done for this measurement.

The uncontrolled measurements from Figure 4.4 are not the same. Notably is a degradation in uncontrolled phase noise seen as K_i increases. This correlation is probably caused by some other environmental effect resulting in the uncontrolled case achieving different comb states for different measurements. The measurements are taken in increasing order of K_i and the comb was tuned to a low noise state at the start of the measurement sequence. This means that the uncontrolled comb started in a low noise state, in the top left figure, to then degrade as time passed to a higher noise state which is seen in the bottom right part of Figure 4.4. None of the measurements is more true than any other as the uncontrolled comb drifts between different states throughout normal operation. The drift of the uncontrolled comb should be taken into consideration when performing long term measurements of uncontrolled combs.

4.4 Reference oscillator

Equation 3.1 shows the relation between reference oscillator and measured repetition rate. The equation implies that drift and phase noise from the reference oscillator is multiplied by the factor n before affecting the measurement $n = 2 = 3\,\text{dB}$ combs were used in this thesis.

The change in frequency of the utilized reference oscillator for OEDC was measured and the results are shown in Figure 4.5.

Figure 4.5 contains what could be an exponential decrease. This could also be explained by thermal effects as people entered and left the room causing a change in temperature. These effects are sufficiently small to be discarded as an error source for the long term measurements presented in this thesis. However, if OEDC is to be used for more accurate combs, then a thermal controller should be used for the reference oscillator.

The phase noise of the reference oscillator was measured and the result is shown in Figure 4.6. The phase noise of the oscillator is much lower than the phase noise of the uncontrolled and controlled comb (see Figure 4.3) for low offset frequencies. For those frequencies, it is concluded that the controller compensates for noise in the system. For large offsets is the phase noise of the reference lower than that of the comb. However, more stable combs, or combs with larger repetition rates, will soon be limited by the phase noise of the reference.

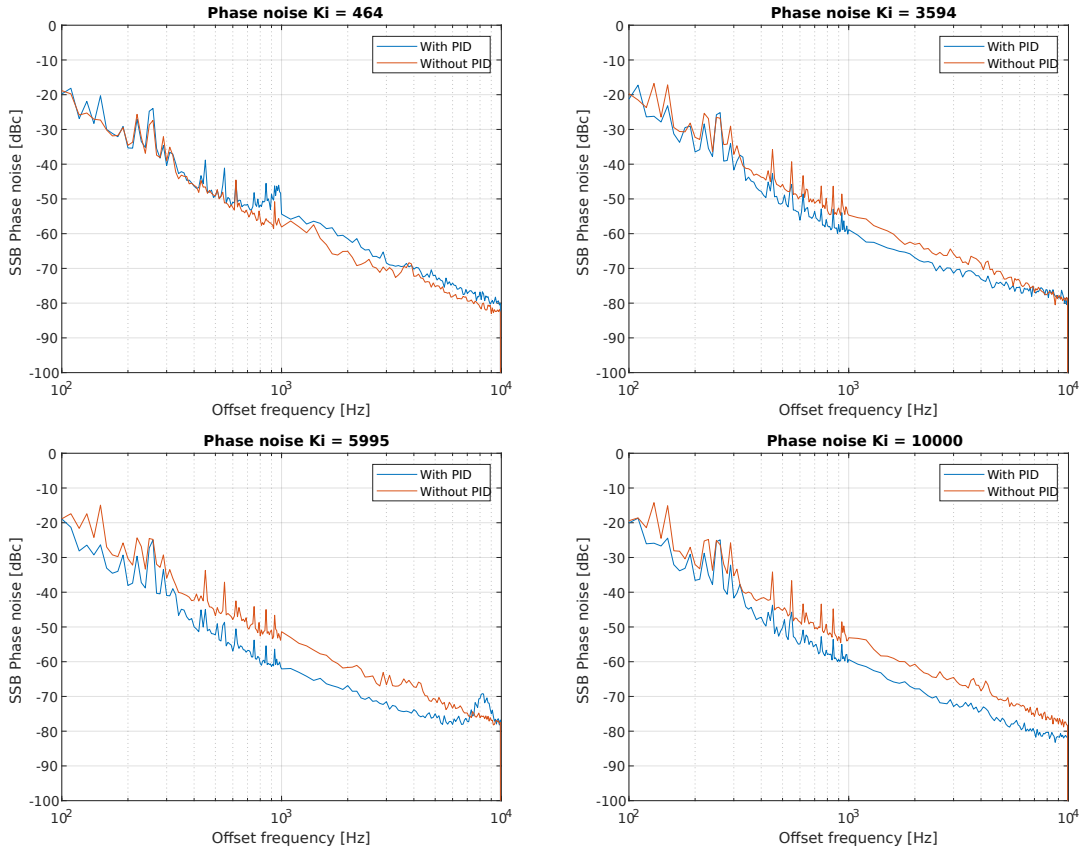

Figure 4.4: Comparison of phase noise performance for four different values of K_i. Images show different behaviors. Bottom and top left figures contains an oscillation which is visualized as a peak in phase noise. All figures show a degradation in phase noise from the controlled case after the integrating bandwidth of the controller. Different K_i are shown to correspond to different uncontrolled phase noise plots.

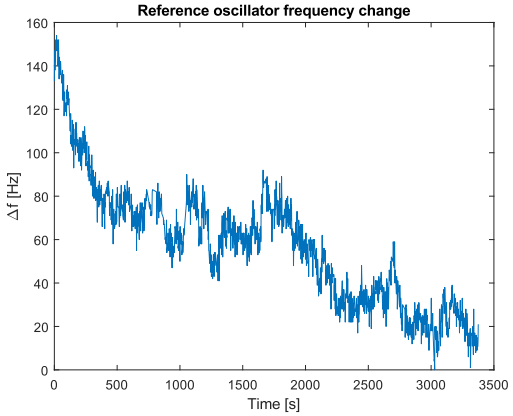

Figure 4.5: Measurement of the reference oscillator stability used for OEDC. A total variation of 150 Hz peak to peak is achieved for a 25.1 GHz oscillator.

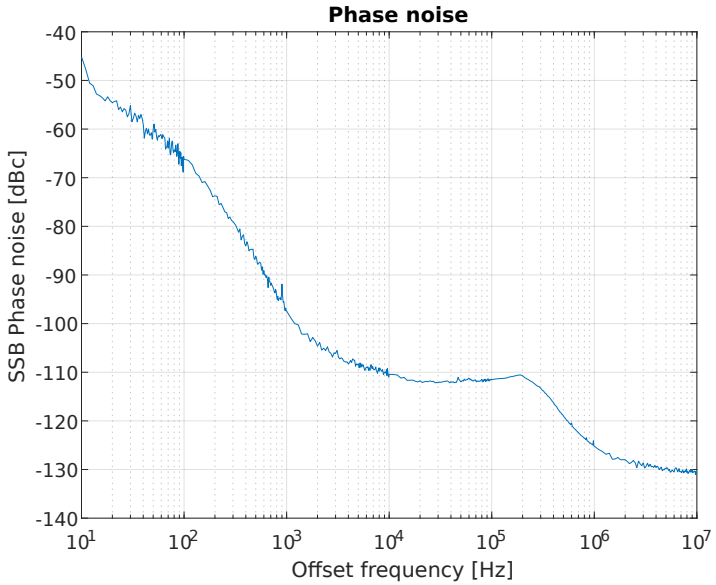

Figure 4.6: Reference oscillator single side band phase noise. It is lower than the measured phase noise of the comb for all frequencies.

4.5 Compensating for coupler drift

The performance of the coupling controller was evaluated without an active comb. Figure 4.7 compares the coupling losses with and without the coupling controller. The controlled losses decrease at the start of the experiment because the coupling was not optimal before starting the measurements. In contrast, the uncontrolled experiment started right after the controlled one and was therefore optimally coupled from the start. Steady state noise is similar between the two measurements. The uncontrolled losses begin to increase significantly halfway through the experiment while the controlled case remains constant.

Both experiments have significant variations in loss around the 2500 s point. The timing of these variations is purely a coincidence as the experiments were performed back to back and were not exposed to the same environmental effects.

The start of the controlled measurement shows a decrease in losses. This is the controller compensating for a sub-optimal coupling. However, the controller is not able to do this reliably for large errors in initial coupling. It is likely to get stuck in a local minimum in coupling strength. This is not an issue as finding the initial maximum only takes a few minutes manually.

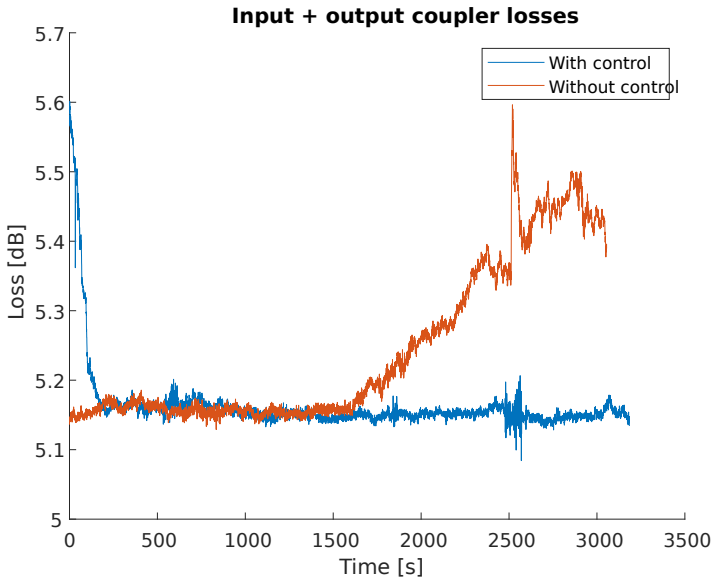

Figure 4.7: Coupling losses with and without the transmitted power maximization algorithm enabled. No comb is present in the device. The uncontrolled system starts drifting halfway through the experiment while the controlled one remains constant. Experiments are performed back to back with the controlled one running first.

5

Conclusion

A photonic molecule microcomb was stabilized by active feedback control of the detuning. Detuning was measured indirectly as soliton power and altered by moving the longitudinal mode of the cavity thermally. This control scheme increases the long-term stability of the comb as well as decreases its phase noise within the bandwidth of the controller.

This result enables future research around photonic molecule microcombs by decreasing their phase noise, increasing their lifespan and thus the length of an experiment as well as reducing their sensitivity to external forces such as acoustic vibrations and temperature.

These improvements facilitate the further development of photonic molecule microcomb towards applications such as spectroscopy, optical telecommunication and metrology. To achieve these long term goals more research is needed within stabilization of the photonic molecule microcomb. The sections below outline such future research.

5.1 Coupling stability

The stability of a photonic molecule microcomb controlled by locking the converted power to a constant value seemed limited by coupling stability. Further research should go towards eliminating coupling drift from the equation by proper packaging as done in [45] or active control of the coupling stages as demonstrated in this thesis. The purpose of that research is to achieve as low drift as possible as well as investigate if the measured correlation between transmitted power and repetition rate is caused by coupling drift.

5.2 Phase noise measurement method

The method used for measuring phase noise, OEDC, requires a stable, high power and high frequency reference oscillator. These three things are difficult to engineer into the same oscillator and thus the accuracy of the measurements in this thesis is limited by the oscillator at hand. Future work into control of combs should consider a direct detection scheme of the repetition rate using faster photodiodes and spectrum analyzers. Purchasing another reference seems futile as last year's

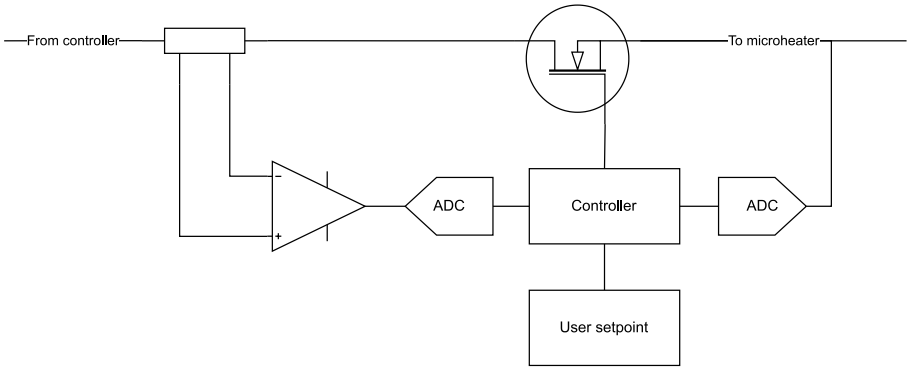

Figure 5.1: Block diagram of overpower protection. It protects the microheaters by multiplying the digitized voltage and current inputs and comparing the product to a user set point.

model of high frequency signal generator from Keysight has similar phase noise performance at a lower output power [46] when compared to the available oscillator.

OEDC also provides poor optical signal to noise ratio at the photodiode before the phase noise analyzer. This is because significant comb power is lost during modulation. A high optical signal to noise ratio is needed to avoid the shot noise limit of the PD. Compensation for this requires extra RF and optical amplifiers as well as optical filters which introduces extra complexity and noise sources.

Direct detection, in which the the repetition rate is detected with a single sufficiently fast photodiode is also possible. This works around the two aforementioned issues but requires a fast photodiode or comb with a low repetition rate as used by [47].

5.3 Heater robustness

The microheaters found on the photonic molecules, which can be seen in Figure 1.1, are quite fragile and breaking one makes a device unusable. I broke quite a few during this thesis. A few paths could be explored to improve the heaters. One of them is the design of the heaters where the interesting design parameters are maximum power capability and bandwidth. The distribution of these parameters could also be investigated as a power that broke one of my heaters did not break another.

An electronic power limiter could also be explored. It should measure current through and voltage across the heater, multiply them and introduce a large series resistance via a, for instance, series transistor if the power reaches a set point. A schematic sketch of such a system is shown in Figure 5.1. The bandwidth of its control system could be similar to the heater bandwidth, about 100 kHz. However, I've only destroyed heaters when initiating a comb manually. Thus a smaller bandwidth, say 1 kHz, could be used to grant protection from the user of the comb. The pass transistor should be dimensioned such that the heater bandwidth is unaffected.

5.4 Locking to a frequency reference

Locking the output spectrum to a converted power set point has shown to significantly improve both stability and phase noise. However, better performance could probably be achieved by locking to a frequency reference as it directly measures and compensates for variations in the parameter of interest, the repetition rate.

5.5 Requirements on control system

The utilized controller, the RP [31], is significantly over-dimensioned for the control system. A smaller, cheaper and lower power with a higher digital resolution solution could be constructed from audio grade signal converters and a micro controller or smaller FPGA. Such a system would be more suitable for use in consumer applications. However, the phonoic molecules are not yet sufficiently mature for commercial deployment meaning that the cost of an over-dimensioned system is negligible.

Bibliography

[1] S. A. Diddams, K. Vahala, and T. Udem, "Optical frequency combs: coherently uniting the electromagnetic spectrum," *Science*, vol. 369, no. 6501, 2020.

[2] T. W. Hänsch, "Nobel lecture: passion for precision," *Reviews of Modern Physics*, vol. 78, no. 4, p. 1297, 2006.

[3] T. J. Kippenberg, R. Holzwarth, and S. A. Diddams, "Microresonator-based optical frequency combs," *science*, vol. 332, no. 6029, pp. 555–559, 2011.

[4] H. Margolis, "Timekeepers of the future," *Nature Physics*, vol. 10, no. 2, pp. 82–83, 2014.

[5] T. Udem, R. Holzwarth, and T. W. Hänsch, "Optical frequency metrology," *Nature*, vol. 416, no. 6877, pp. 233–237, 2002.

[6] S. Schiller, "Spectrometry with frequency combs," *Optics letters*, vol. 27, no. 9, pp. 766–768, 2002.

[7] V. Gerginov, C. E. Tanner, S. Diddams, A. Bartels, and L. Hollberg, "Optical frequency measurements of $6s^2S_{1/2} - 6p^2P_{3/2}$ transition in a ^{133}Cs atomic beam using a femtosecond laser frequency comb," *Physical Review A*, vol. 70, no. 4, p. 042505, 2004.

[8] R. Holzwarth, A. Y. Nevsky, M. Zimmermann, T. Udem, T. Hänsch, J. Von Zanthier, H. Walther, J. Knight, W. Wadsworth, P. S. J. Russell *et al.*, "Absolute frequency measurement of iodine lines with a femtosecond optical synthesizer," *Applied Physics B*, vol. 73, no. 3, pp. 269–271, 2001.

[9] T. Steinmetz, T. Wilken, C. Araujo-Hauck, R. Holzwarth, T. W. Hänsch, L. Pasquini, A. Manescau, S. D'odorico, M. T. Murphy, T. Kentischer *et al.*, "Laser frequency combs for astronomical observations," *Science*, vol. 321, no. 5894, pp. 1335–1337, 2008.

[10] W. Liang, D. Eliyahu, V. S. Ilchenko, A. A. Savchenkov, A. B. Matsko, D. Seidel, and L. Maleki, "High spectral purity Kerr frequency comb radio frequency photonic oscillator," *Nature communications*, vol. 6, no. 1, pp. 1–8, 2015.

[11] I. Coddington, W. C. Swann, and N. R. Newbury, "Coherent multiheterodyne spectroscopy using stabilized optical frequency combs," *Physical Review Letters*, vol. 100, no. 1, p. 013902, 2008.

[12] T. Ideguchi, S. Holzner, B. Bernhardt, G. Guelachvili, N. Picqué, and T. W. Hänsch, "Coherent Raman spectro-imaging with laser frequency combs," *Nature*, vol. 502, no. 7471, pp. 355–358, 2013.

[13] I. Coddington, N. Newbury, and W. Swann, "Dual-comb spectroscopy," *Optica*, vol. 3, no. 4, pp. 414–426, 2016.

[14] A. Fülöp, M. Mazur, A. Lorences-Riesgo, T. A. Eriksson, P.-H. Wang, Y. Xuan, D. E. Leaird, M. Qi, P. A. Andrekson, A. M. Weiner *et al.*, "Long-haul coherent communications using microresonator-based frequency combs," *Optics express*, vol. 25, no. 22, pp. 26 678–26 688, 2017.

[15] P. Marin-Palomo, J. N. Kemal, M. Karpov, A. Kordts, J. Pfeifle, M. H. Pfeiffer, P. Trocha, S. Wolf, V. Brasch, M. H. Anderson *et al.*, "Microresonator-based solitons for massively parallel coherent optical communications," *Nature*, vol. 546, no. 7657, pp. 274–279, 2017.

[16] A. Fülöp, M. Mazur, A. Lorences-Riesgo, Ó. B. Helgason, P.-H. Wang, Y. Xuan, D. E. Leaird, M. Qi, P. A. Andrekson, A. M. Weiner *et al.*, "High-order coherent communications using mode-locked dark-pulse Kerr combs from microresonators," *Nature communications*, vol. 9, no. 1, pp. 1–8, 2018.

[17] MenloSystems. (2022) Smartcomb compact optical frequency comb. [Online]. Available: https://www.menlosystems.com/products/optical-frequency-combs/smartcomb/

[18] P. Del'Haye, A. Schliesser, O. Arcizet, T. Wilken, R. Holzwarth, and T. J. Kippenberg, "Optical frequency comb generation from a monolithic microresonator," *Nature*, vol. 450, no. 7173, pp. 1214–1217, 2007.

[19] T. J. Kippenberg, A. L. Gaeta, M. Lipson, and M. L. Gorodetsky, "Dissipative Kerr solitons in optical microresonators," *Science*, vol. 361, no. 6402, 2018.

[20] C. Bao, L. Zhang, A. Matsko, Y. Yan, Z. Zhao, G. Xie, A. M. Agarwal, L. C. Kimerling, J. Michel, L. Maleki *et al.*, "Nonlinear conversion efficiency in Kerr frequency comb generation," *Optics letters*, vol. 39, no. 21, pp. 6126–6129, 2014.

[21] X. Xue, P.-H. Wang, Y. Xuan, M. Qi, and A. M. Weiner, "Microresonator Kerr frequency combs with high conversion efficiency," *Laser & Photonics Reviews*, vol. 11, no. 1, p. 1600276, 2017.

[22] Ó. B. Helgason, F. R. Arteaga-Sierra, Z. Ye, K. Twayana, P. A. Andrekson, M. Karlsson, J. Schröder, and V. Torres-Company, "Dissipative solitons in photonic molecules," *Nature Photonics*, vol. 15, no. 4, pp. 305–310, 2021.

[23] T. Herr, V. Brasch, J. D. Jost, C. Y. Wang, N. M. Kondratiev, M. L. Gorodetsky, and T. J. Kippenberg, "Temporal solitons in optical microresonators," *Nature Photonics*, vol. 8, no. 2, pp. 145–152, 2014.

[24] T. Herr, K. Hartinger, J. Riemensberger, C. Wang, E. Gavartin, R. Holzwarth, M. Gorodetsky, and T. Kippenberg, "Universal formation dynamics and noise of Kerr-frequency combs in microresonators," *Nature photonics*, vol. 6, no. 7, pp. 480–487, 2012.

[25] M. Zhang, C. Wang, Y. Hu, A. Shams-Ansari, T. Ren, S. Fan, and M. Lončar, "Electronically programmable photonic molecule," *Nature Photonics*, vol. 13, no. 1, pp. 36–40, 2019.

[26] X. Xue, X. Zheng, and B. Zhou, "Super-efficient temporal solitons in mutually coupled optical cavities," *Nature Photonics*, vol. 13, no. 9, pp. 616–622, 2019.

[27] X. Yi, Q.-F. Yang, K. Y. Yang, M.-G. Suh, and K. Vahala, "Soliton frequency comb at microwave rates in a high-Q silica microresonator," *Optica*, vol. 2, no. 12, pp. 1078–1085, 2015.

[28] A. Fülöp, P.-H. Wang, Y. Xuan, D. E. Leaird, M. Qi, P. A. Andrekson, A. M. Weiner, and V. Torres-Company, "Active feedback stabilization of normal-dispersion microresonator combs," in *2017 Conference on Lasers and Electro-Optics Europe & European Quantum Electronics Conference (CLEO/Europe-EQEC)*. IEEE, 2017, pp. 1–1.

[29] X. Yi, Q.-F. Yang, K. Y. Yang, and K. Vahala, "Active capture and stabilization of temporal solitons in microresonators," *Optics letters*, vol. 41, no. 9, pp. 2037–2040, 2016.

[30] P. Del'Haye, O. Arcizet, A. Schliesser, R. Holzwarth, and T. J. Kippenberg, "Full stabilization of a microresonator-based optical frequency comb," *Physical Review Letters*, vol. 101, no. 5, p. 053903, 2008.

[31] STEMlab. (2022) Stemlab 125-14. [Online]. Available: https://redpitaya.com/stemlab-125-14/

[32] Z. Ye, A. Fülöp, Ó. B. Helgason, P. A. Andrekson *et al.*, "Low-loss high-Q silicon-rich silicon nitride microresonators for Kerr nonlinear optics," *Optics letters*, vol. 44, no. 13, pp. 3326–3329, 2019.

[33] T. Carmon, L. Yang, and K. J. Vahala, "Dynamical thermal behavior and thermal self-stability of microcavities," *Optics express*, vol. 12, no. 20, pp. 4742–4750, 2004.

[34] A. Arbabi and L. L. Goddard, "Measurements of the refractive indices and thermo-optic coefficients of Si_3N_4 and SiOx using microring resonances," *Optics letters*, vol. 38, no. 19, pp. 3878–3881, 2013.

[35] S. Kim, K. Han, C. Wang, J. A. Jaramillo-Villegas, X. Xue, C. Bao, Y. Xuan, D. E. Leaird, A. M. Weiner, and M. Qi, "Dispersion engineering and frequency comb generation in thin silicon nitride concentric microresonators," *Nature communications*, vol. 8, no. 1, pp. 1–8, 2017.

[36] F. Lei, Z. Ye *et al.*, "Thermal noise reduction in soliton microcombs via laser self-cooling," *Optics Letters*, vol. 47, no. 3, pp. 513–516, 2022.

[37] G. Huang, E. Lucas, J. Liu, A. S. Raja, G. Lihachev, M. L. Gorodetsky, N. J. Engelsen, and T. J. Kippenberg, "Thermorefractive noise in silicon-nitride microresonators," *Physical Review A*, vol. 99, no. 6, p. 061801, 2019.

[38] C. Bao, Y. Xuan, C. Wang, J. A. Jaramillo-Villegas, D. E. Leaird, M. Qi, and A. M. Weiner, "Soliton repetition rate in a silicon-nitride microresonator," *Optics letters*, vol. 42, no. 4, pp. 759–762, 2017.

[39] X. Yi, Q.-F. Yang, X. Zhang, K. Y. Yang, X. Li, and K. Vahala, "Single-mode dispersive waves and soliton microcomb dynamics," *Nature communications*, vol. 8, no. 1, pp. 1–9, 2017.

[40] T. Labs. (2022) 3-axis nanomax flexure stage with bundled controller. [Online]. Available: https://www.thorlabs.com/newgrouppage9.cfm?objectgroup_id=1098

[41] ——. (2022) DX50AF - single mode ultrafast detector module, 1250 - 1650 nm, dc - 50 ghz, fc/pc. [Online]. Available: https://www.thorlabs.com/thorproduct.cfm?partnumber=DX50AF

[42] P. Del'Haye, S. B. Papp, and S. A. Diddams, "Hybrid electro-optically modulated microcombs," *Physical review letters*, vol. 109, no. 26, p. 263901, 2012.

[43] C. Joshi, J. K. Jang, K. Luke, X. Ji, S. A. Miller, A. Klenner, Y. Okawachi, M. Lipson, and A. L. Gaeta, "Thermally controlled comb generation and soliton modelocking in microresonators," *Optics letters*, vol. 41, no. 11, pp. 2565–2568, 2016.

[44] M. A. Luda, M. Drechsler, C. T. Schmiegelow, and J. Codnia, "Compact embedded device for lock-in measurements and experiment active control," *Review of Scientific Instruments*, vol. 90, no. 2, p. 023106, 2019.

[45] J. Nauriyal, M. Song, R. Yu, and J. Cardenas, "Fiber to chip fusion splicing for robust, low loss photonic packaging," *arXiv preprint arXiv:1810.09531*, 2018.

[46] Keysight. (2021) E8267d psg vector signal generator. [Online]. Available: https://www.keysight.com/se/en/assets/7018-01210/data-sheets/5989-0697.pdf

[47] Z. Ye, F. Lei, K. Twayana, M. Girardi, P. A. Andrekson, and V. Torres-Company, "Integrated, ultra-compact high-Q silicon nitride microresonators for low-repetition-rate soliton microcombs," *Laser & Photonics Reviews*, vol. 16, no. 3, p. 2100147, 2022.

A

Working with PID and photonic molecule microcombs

This appendix is intended as documentation for the researchers wanting to use the control methods developed in this thesis for future work with microcombs. It describes how the RP is used and pitfalls that I ran into.

A.1 Control software

Two methods have been used. One is the lock-in+PID[1] the other is using pyrpl[2]. The user interface of lock-in is in my opinion better than that of pyrpl. However pyrpl has a few technical advantages. It is able to be interfaced with via python and enables more flexible analysis of the signals by running an oscilloscope and spectrum analyser at the same time as the PID controller. However, it is also limited in some manners. Firstly, there is no K_d available in the pyrpl controller even though the module is called PID and secondly is the maximum value of K_i limited to a few tens of kHz. None of these limitations are present in the lock-in controller. These limitations are not significant as K_d can be left unused in a lot of cases and the limited K_i matters little as the heaters are unable to operate over 100 kHz. I would therefor recommend pyrpl.

Using pyrpl is a three step process. First open the pyrpl software, called pyrpl-windows, and navigate to the PID module. Make sure that $K_i, K_p = 0$, $I_{val} = 0$ and that the correct inputs and outputs are selected. The PID controller is now disabled and the comb can be initiated. Second, verify the relation between converted power and heater voltage, what I write here applies when there is a π phase between converted power and heater voltage, i.e an increase in heater voltage decreases the converted power and set a set point for the converted power. The set point as entered in the user interface is the voltage to lock the converted power to. You are now able to enter K_p and K_i which should be positive. $0.01 < K_p < 2$, $K_i < 10000$ has worked well for me just make sure that there are no oscillations. The scope app of the pyrpl works well for this observation. The spectrum of the input signal can be observed in the spectrum analyser module to see how the controller attenuates errors. The controller is working properly if the input is attenuated for $f < K_i$.

[1] `https://marceluda.github.io/rp_lock-in_pid/`
[2] `https://pyrpl.readthedocs.io/en/latest/`

Third should the PID module be closed in the user interface in order to allow python to access the module. The python script will fail to interface with the RP once however the second attempt has always worked for me.

Be careful about using the arrow keys to change PID parameters. The user interface has a velocity based control which I find counterintuitive to use. Every time I tried using the arrow keys to tweak parameters I lost the comb.

A.2 Optical filter

A narrow band and steep optical filter for selecting the comb lines for the converted power is needed if the best stability is required. A wider filter makes the system more sensitive to state changes that redistribute the converted power between the lines. The effect of different filter sizes is investigated more in the thesis itself.

The stop band attenuation of the filter is also of importance. If a few lines are used for measurement must those lines be selected close to the pump to have significant power for detection. The stop band attenuation of the filter therefore sets the amount of pump power seen in the converted power measurement. As the detuning increases is the converted power increasing (equation 2.10) however the pump power transmitted through the resonator decreases as more power gets coupled into resonance. Leakage between pump and converted power measurement therefore reduces the sensitivity of the measured power to the detuning.